A&A 576, A48 (2015)
DOI: 10.1051/0004-6361/201424965

Astronomy & Astrophysics

The HARPS search for southern extra-solar planets

XXXVII. Five new long-period giant planets and a system update⋆,⋆⋆

C. Moutou[1,2], G. Lo Curto[3], M. Mayor[4], F. Bouchy[2], W. Benz[5], C. Lovis[4], D. Naef[4], F. Pepe[4], D. Queloz[4], N. C. Santos[6,7], D. Ségransan[4], S. G. Sousa[6,7], and S. Udry[4]

[1] Canada France Hawaii Telescope Corporation, Kamuela 96743, USA
e-mail: moutou@cfht.hawaii.edu
[2] Aix Marseille Université, CNRS, LAM (Laboratoire d'Astrophysique de Marseille) UMR 7326, Marseille, France
[3] ESO, Alonso de Córdova 3107, Vitacura, Casilla 19001, Santiago de Chile, Chile
[4] Observatoire de Genève, Université de Genève, 51 chemin des Maillettes, 1290 Sauverny, Switzerland
[5] Physikalisches Institut Universität Bern, Sidlerstrasse 5, 3012 Bern, Switzerland
[6] Instituto de Astrofísica e Ciências do Espaco, Universidade do Porto, CAUP, Rua das Estrelas, 4150-762 Porto, Portugal
[7] Centro de Astrofísica e Departamento de Física e Astronomia, Faculdade de Ciências, Universidade do Porto, Rua das Estrelas, 4150-762 Porto, Portugal

Received 12 September 2014 / Accepted 9 December 2014

ABSTRACT

We describe radial-velocity time series obtained by HARPS on the 3.60 m telescope in La Silla (ESO, Chile) over ten years and report the discovery of five new giant exoplanets in distant orbits; these new planets orbit the stars HD 564, HD 30669, HD 108341, and BD -114672. Their periods range from 492 to 1684 days, semi-major axes range from 1.2 to 2.69 AU, and eccentricities range from 0 to 0.85. Their minimum mass ranges from 0.33 to 3.5 $M_{\rm Jup}$. We also refine the parameters of two planets announced previously around HD 113538, based on a longer series of measurements. The planets have a period of 663 ± 8 and 1818 ± 25 days, orbital eccentricities of 0.14 ± 0.08 and 0.20 ± 0.04, and minimum masses of 0.36 ± 0.04 and 0.93 ± 0.06 $M_{\rm Jup}$. Finally, we report the discovery of a new hot-Jupiter planet around an active star, HD 103720; the planet has a period of 4.5557 ± 0.0001 days and a minimum mass of 0.62 ± 0.025 $M_{\rm Jup}$. We discuss the fundamental parameters of these systems and limitations due to stellar activity in quiet stars with typical 2 m s^{-1} radial velocity precision.

Key words. planetary systems – techniques: radial velocities – techniques: spectroscopic – methods: observational

1. Introduction

Thanks to radial-velocity (RV) surveys collecting data since more than 20 years, on one hand, and advanced technologies in high-contrast imaging, on the other hand, the parameter spaces of exoplanets discovered by these two methods are now joined in the regime of massive planets (Fig. 1). Both exoplanet populations rejoin at a semi-major axis of 8−10 AU (i.e., at Saturn's orbit). The types of stars around which these exoplanets are discovered, however, differ much as a result of the detection bias of these two methods: quiet, FGKM stars are more favorable to RV survey stars, and very young (hence, active) nearby stars to direct imaging surveys, these last ones being mostly of AF spectral types. This complementarity is important for obtaining a global architecture of planetary systems and constrain a planet formation scenario, and some overlap is essential to calibrate measured quantities, especially the mass, since it is inferred from photometric measurements in the case of imaged systems (e.g., Spiegel & Burrows 2012; Allard et al. 2013). With new upcoming instruments such as GPI (Macintosh et al. 2008) and SPHERE (Beuzit et al. 2008), more giant planets in the 5−10 AU range will be discovered, some of which will hopefully have a corresponding signature in the RV parameter space, which will allow a gravitational estimate on the planet mass in addition to the spectrophotometric characterization from direct imaging.

In a similar way to how speckles limit the contrast at which a planet can be directly imaged, the search for long-period exoplanets in RV surveys suffers from another noise due to the host star, with activity at the stellar surface generating a RV jitter (e.g., Saar et al. 1998; Wright 2005; Boisse et al. 2011; Dumusque et al. 2011). With the amplitude of the Doppler wobble decreasing with the orbital distance, even giant planets have signatures whose amplitude can be buried in stellar noise, given that activity-driven RV noise has multiple frequency components, including the one due to several-year long magnetic cycles (Santos et al. 2010). To correct for stellar activity, very high precision on the usual diagnostics parameters is needed: full width at half maximum (FWHM) and bisector span of the stellar cross-correlation function, and the CaII index.

In this paper, we present four new giant planets discovered by the RV spectrograph HARPS in the volume-limited survey (Lo Curto et al. 2010) and discuss their properties: the hot-Jupiter HD 103720 b, and long-period giant planets around HD 564, HD 30669, and HD 108341. In addition, we update the analysis of two systems: HD 113538, composed of two planets

⋆ Based on observations made with the HARPS instrument on the ESO 3.6 m telescope at La Silla (Chile), under the GTO program ID 072.C-0488, 183.C-0972 and the regular programs: 085.C-0019, 087.C-0831, 089.C-0732, 090.C-0421, 091.C-0034, and 092.C-0721.

⋆⋆ Figures 8 and 9 and Tables 4–9 are available in electronic form at http://www.aanda.org

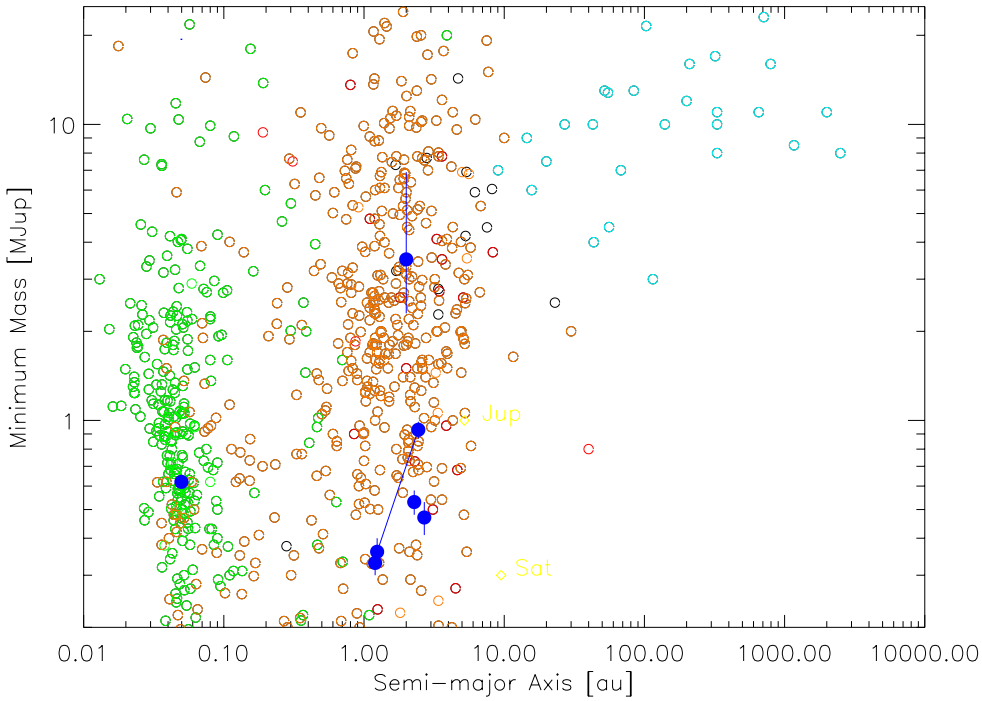

Fig. 1. Semi-major axis versus projected mass for planets farther than 0.01 AU and more massive than 0.2 $M_{\rm Jup}$. The symbol color indicates the discovery method (blue: direct imaging; orange: RV; green: transits; black: microlenses).

Table 1. Observed and inferred stellar parameters for the planet-hosting stars presented here.

Parameter		HD 103720	HD 564	HD 30669	HD 108341	HD 113538	BD -114672
Sp		K3 V	G2/G3 V	G9 V	K2 V	K9 V	K7 V
V	[mag]	9.49	8.29	9.11	9.36	9.057	9.99
$B-V$	[mag]	0.95	0.61	0.82	0.93	1.376	1.22
π	[mas]	24.05 (1.20)	18.64 (0.88)	17.51 (1.2)	20.23 (0.93)	63.03 (1.36)	36.65 (1.73)
d	[pc]	41.6	53.6	57.1	49.4	15.9	27.3
$T_{\rm eff}$	[K]	5017 (88)	5902 (61)	5400 (74)	5122 (79)	4462 (145)	4475 (100)
log g	[cgs]	4.43 (0.16)	4.53 (0.10)	4.37 (0.55)	4.45 (0.14)	3.79 (0.53)	4.10 (0.36)
[Fe/H]	[dex]	–0.02 (0.06)	–0.20 (0.05)	0.13 (0.06)	0.04 (0.06)	–0.24 (0.06)	–0.48 (0.05)
M_*	[$M_\odot$]	0.794 (0.040)	0.961 (0.050)	0.92 (0.03)	0.843 (0.024)	0.585 (0.05)	0.571 (0.014)
$v \sin i$	[km s^{-1}]	0.42	<2	1.7	<2	<2	<2
min/max S_{MW}		0.49/0.62	0.12/0.22	0.12/0.20	0.10/0.27	0.81/1.34	0.62/0.98
min/max log $R'_{\rm HK}$		–4.53/–4.43	–5.41/–4.68	–5.24/–4.88	–5.30/–4.81	–	–
Age	[Gy]	3.8 (3.7)	5.5 (3.1)	4.8 (4.0)	4.9 (4.1)	4.3 (4.0)	4.4 (4.0)
R_*	[$R_\odot$]	0.73 (0.02)	1.01 (0.05)	0.91 (0.04)	0.79 (0.03)	0.53 (0.02)	0.52 (0.02)
$P_{\rm rot}$	[d]	17	10	35	28	–	–

Notes. For stars with lowest masses, the relationships that derive the activity index log $R'_{\rm HK}$ and the projected velocity are not reliable, so no value is given.

for which the best-fit parameters are refined, and BD -114672, whose signal was previously identified to be due to a long-term magnetic cycle (Moutou et al. 2011). Host stars are described in Sect. 2, radial-velocity observations and analyses in Sect. 3, and Sect. 4 presents a discussion of these new results.

2. Characteristics of the host stars

Because they are part of the volume-limited HARPS survey, all stars presented in this analysis are less than 57.5 pc away from the Sun. This particular sample is composed of six medium-age G and K stars.

The spectroscopic analysis was performed on the combined HARPS spectra by measuring a set of FeI and FeII weak lines with the code ARES (Sousa et al. 2007) and was then used in an homogeneous spectroscopic analysis (e.g., Sousa et al. 2008). For all stars except HD 113538 and BD -114672, the stellar parameters ($T_{\rm eff}$, log g, and [Fe/H]) were taken from the catalog of Sousa et al. (2011). The HIPPARCOS parallaxes of van Leeuwen (2007) were used for the luminosity estimation, and finally, mass, radius, and age of the stars were derived from comparisons with theoretical tracks with a Bayesian analysis[1] (da Silva et al. 2006). All parameters are listed in Table 1. For HD 113538 and BD -114672, updates are provided for the spectroscopic analysis, and in addition, masses (and radii and ages) have been corrected from the erroneous values given in Moutou et al. (2011); these incorrect mass values were due to missing information in

[1] http://stev.oapd.inaf.it/cgi-bin/param

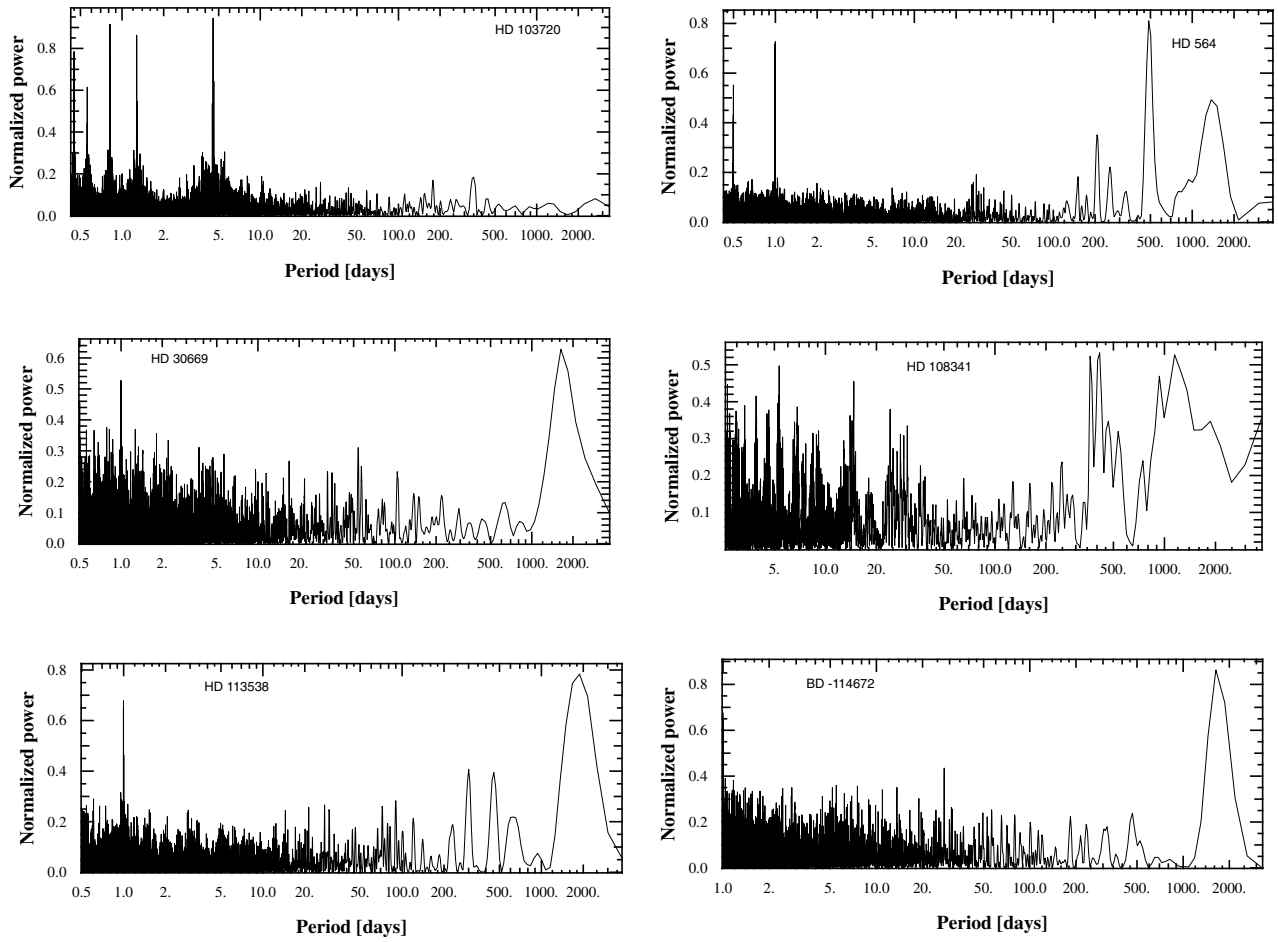

Fig. 2. Periodogram of ten-year HARPS observations.

the evolutionary track interface for low-mass stars, which are solved now (Chen et al. 2014).

Activity indicators (S_{MW} and $\log R'_{\rm HK}$) were individually estimated on each spectrum, and their range of values is given in Table 1. Rotation periods of the stars were estimated from their correlations with the chromospheric activity, as described in Noyes et al. (1984), Mamajek & Hillenbrand (2008). HD 30669 and HD 108341 were less affected by chromospheric activity during these past ten years.

3. Radial velocity data and proposed solutions

Radial-velocity data time series were secured with the spectrograph HARPS, which is mounted full time on the 3.60 m telescope in La Silla, ESO, Chile. The spectrograph is kept in the vacuum under strict temperature control and is fed by an optical fiber with a one-arcsec on-sky aperture. HARPS (Mayor et al. 2003) was used in the HAM mode, allowing the highest resolving power of 115 000, without simultaneous lamp calibration. The observations were conducted in the context of the volume-limited program (Lo Curto et al. 2010), using a precision of about 2 m s^{-1} per measurement in the search for systems containing giant planets. Journals of the observations and RV values are reported in Tables 4 to 9. We secured 70, 99, 46, 24, 75, and 40 individual measurements for HD 103720, HD 564, HD 30669, HD 108341, HD 113538, and BD -114672, respectively. Typical signal-to-noise ratio (S/N) values range from 20 to 50, corresponding to individual RV uncertainties of 1 to 3 m s^{-1}.

The data were processed with the HARPS pipeline, including activity-indicator estimates. The radial velocities were obtained by cross-correlation of the spectra with a numerical mask, as first described in Baranne et al. (1996). The mask was adapted to the spectral type of the star, that is, a K5 mask for HD 103720, HD 108341, HD 113538, and BD -114672, and a G2 mask for HD 564 and HD 30669. The bisector span, a reliable activity indicator, was measured using the cross-correlation profile (see method in Queloz et al. 2001), and its errors were estimated to be twice the RV errors. The CaII H and K chromospheric emission was measured in all spectra (as described in, e.g., Lovis et al. 2011) and calibrated to the Mount Wilson S value and, when appropriate, the $\log R'_{\rm HK}$.

The RV time series were then analyzed with the YORBIT software based on a genetic algorithm (Ségransan et al. 2011), and final parameter sets were calculated using a Markov chain Monte Carlo analysis with Metropolis hasting and looped over 500 000 iterations.

The periodograms of the RV observations are shown in Fig. 2 for all targets. Multiple daily and yearly aliases are visible in addition to the signal peak(s). In the following, we discuss our analyses and interpretation of the RV time series for each individual target.

Table 2. Orbital and physical parameters for five planets presented in this paper; median values are shown, and 1σ errors are given in parenthesis.

Parameter		HD 103720 b	HD 564 b	HD 30669 b	HD 108341 b	BD -114672 b
P	[days]	4.5557 (0.0001)	492.3 (2.3)	1684 (61)	1129 (–8, +6)	1667 (–31, +33)
T	[JD-2 454 000]	1387.46 (0.04)	1433 (9)	3181 (–1395, +101)	2633 (–88, +33)	1899 (–46, 38)
e		0.086 (0.024)	0.096 (0.067)	0.18 (0.15)	0.85 (–0.08, +0.09)	0.05 (–0.04, +0.06)
γ	[km s^{-1}]	–6.5 (1.4)	11.46 (0.38)	65.8 (0.8)	56.7 (–4, +3)	–87.3 (0.68)
ω	[deg]	262 (15)	314 (31)	82 (–36, +43)	190 (–5, +2)	231 (–143, +77)
K	[m s^{-1}]	89 (2)	8.79 (0.45)	8.6 (1.1)	144 (–66, +311)	13.4 (1.0)
$a_1 \sin i$	[10^{-3} AU]	0.0371 (0.0008)	0.39 (0.02)	1.30 (0.15)	2.96 (–0.5, +4.2)	2.05 (0.16)
$m_2 \sin i$	[$M_{\rm Jup}$]	0.620 (0.025)	0.33 (0.03)	0.47 (0.06)	3.5 (–1.2, +3.4)	0.53 (0.05)
a	[AU]	0.0498 (0.0008)	1.2 (0.02)	2.69 (0.08)	2.00 (–0.04, +0.04)	2.28 (0.07)
$N_{\rm meas}$		70	99	46	24	40
Span	[days]	3353	4008	3799	3770	3271
σ (O–C)	[m s^{-1}]	13.1	2.9	3.6	1.5	2.9
$\chi^2_{\rm red}$		50	2.2	6.1	1.1	2.7

Notes. T is the epoch of maximum RV. σ(O–C) is the residual noise after orbital fitting of the combined set of measurements.

3.1. HD 103720

The 70 HARPS measurements of star HD 103720 show a variability of 100 m s^{-1}; individual measurements have an average uncertainty of 2 m s^{-1}. Although the star is active, with an average $\log R'_{\rm HK}$ of −4.48 (or S of 0.55), and shows visible variability in the bisector span and CaII individual measurements (Figs. 10 and 11), it is unlikely that activity alone produces such a high RV variation. From calibrations derived between CaII and RV activity jitter (Santos et al. 2000), one expects a jitter of 9 m s^{-1} for a star such as HD 103720, a factor 7 smaller than the RV variability. In addition, neither the bisector span nor the CaII index shows variations at frequency similar to the 4.5-day period of the velocities, and these quantities are not correlated with velocity. The photometric variability of this star is reported in the VSX[2] database as characterized by a 17-day period and a 0.05 mag amplitude (Watson et al. 2014).

When a Keplerian is adjusted to the RV data of HD 103720, the RV variations are compatible with the presence of a sinusoidal wobble of amplitude 89 m s^{-1} that would be produced by a planet of period P = 4.555 days in a circular orbit, and of mass $M_{\rm p}$ = 0.62 $M_{\rm Jup}$. Figure 3 shows the phase-folded data points together with the best-fit solution and the residuals over time. There is no clear periodicity in the residuals when the main Doppler-induced signal is removed. The residual jitter has a root mean square (rms) amplitude of 11 m s^{-1}. It excludes another giant planet of more than 1 $M_{\rm Jup}$ in a 70-day circular orbit, and a 4 $M_{\rm Jup}$ planet in a 3000 day orbit. Since the residuals are compatible with the expected jitter, they are attributed to spot and plage activity at the surface of the star, while the main signal is safely attributed to a giant planet in orbit.

The final parameters of the planet are given in Table 2.

With an orbital period of 4.555 days and a stellar radius of 0.73 $R_\odot$, this giant planet has a 7% probability of transiting the disk of its parent star. All system parameters are given in Table 2. The ephemeris of a transit configuration are T_0 = 2 455 388.709 ± 0.047 and P = 4.5557 ± 0.0001 days. No attempt to search for the transit has been made.

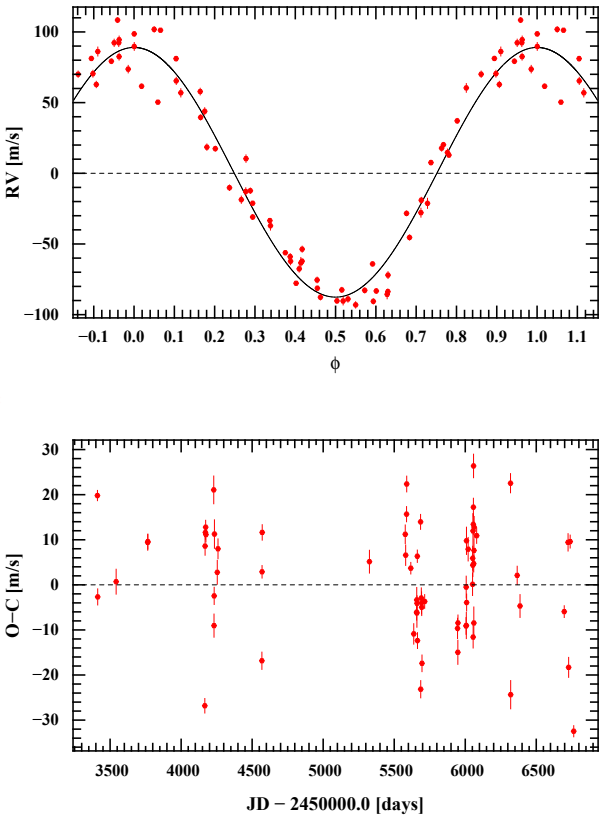

Fig. 3. Radial-velocity measurements of HD 103720 obtained with HARPS against the planet orbital phase together with the best-fit solution (*top*) and the residuals over time (*bottom*).

3.2. HD 564

The metal-poor star HD 564 has been observed during more than ten years with HARPS, during which 99 data points were collected with an average accuracy of 2.5 m s^{-1}. The RV measurements show a variability of 20 m s^{-1} amplitude, or twice the jitter level expected from the chromospheric activity index. The CaII index is not correlated to the RV variations (bottom of Fig. 4). The bisector span varies over a similar range as the velocities, but with a Pearson correlation coefficient of 0.04. Even if the star may show some activity despite its low $\log R'_{\rm HK}$ value, we are confident that activity alone cannot explain the RV variations, because i) we cover nine periods and the power in the RV-periodogram peak at 490 days is very strong over the ten years of monitoring, showing a stable signal; ii) activity indices

[2] http://www.aavso.org/vsx/

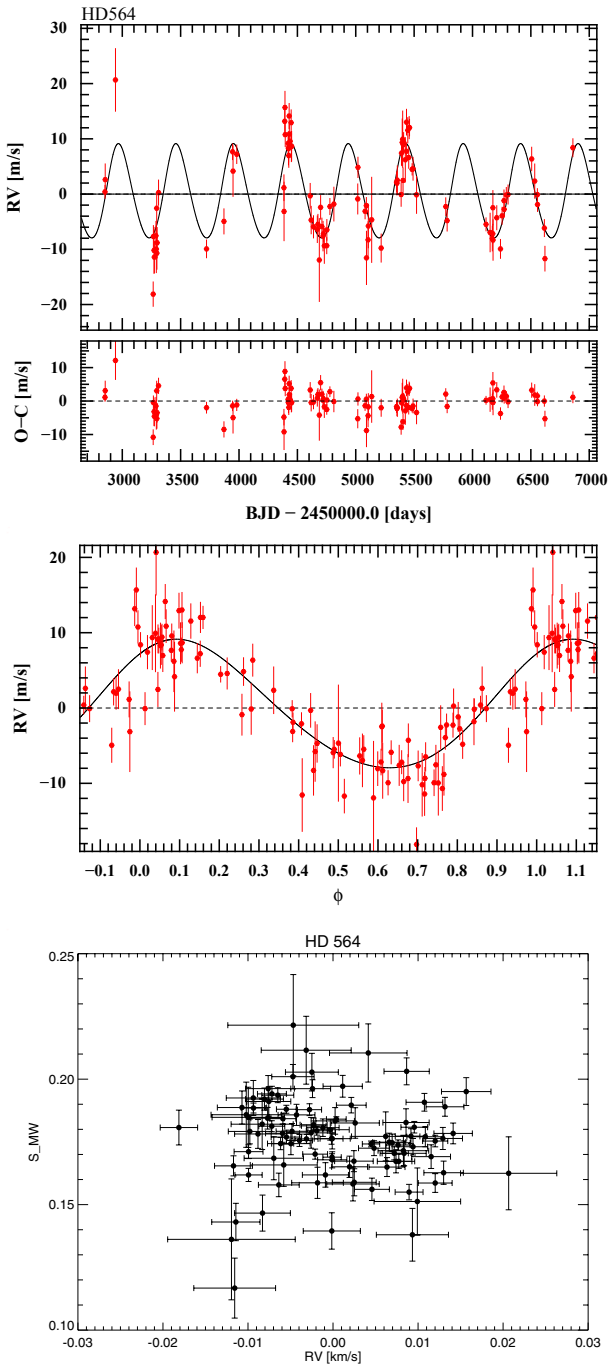

Fig. 4. Radial-velocity measurements of HD 564 obtained with HARPS against time (*top*) and against the planet orbital phase (*middle*) together with the best-fit solution. The CaII index is not correlated with the RV variations (*bottom*).

have power peaks spread over a wider range of periods; iii) there is no correlation between velocities and activity indices.

When a Keplerian is adjusted to the 99 HARPS data points, the best fit has an orbit of 492.3 ± 2.3 days and a semi-amplitude of 8.79 ± 0.45 m s^{-1} (Fig. 4). The rms of the residuals is 2.9 m s^{-1} and the periodogram of the residuals does not show any periodicity. This signal would correspond to a 0.33 $M_{\rm Jup}$ planet at 1.2 AU from its host star (Table 2).

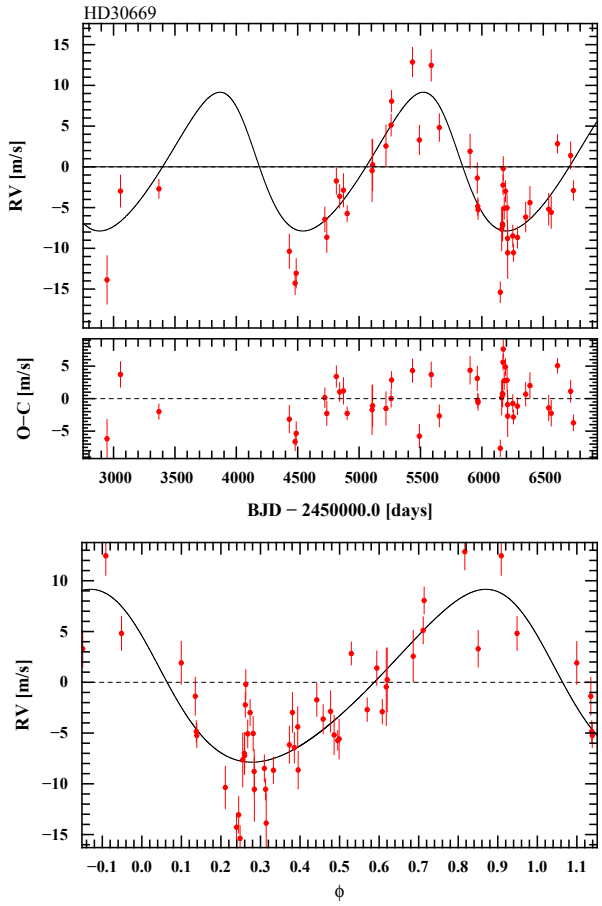

Fig. 5. Radial-velocity measurements of HD 30669 obtained with HARPS against time (*top*) and against the planet orbital phase (*bottom*) together with the best-fit solution.

3.3. HD 30669

The star HD 30669 has been observed 46 times with HARPS over ten years, with an average accuracy of 1.8 m s^{-1}. It is the least active star of the sample described in this work, with an expected velocity jitter of about 7 m s^{-1} due to stellar activity (Santos et al. 2000). The strongest peak in the periodogram of the RV time series lies at about 1680 days. This peak is not present in the periodograms of the CaII index or of the bisector span. Since activity is not an issue, a Keplerian was adjusted to the data, and the best-fit solution corresponds to a signal at a period of 1684 ± 61 days and semi-amplitude 8.6 ± 1.1 m s^{-1} (Fig. 5 and best-fit model parameters in Table 2). The rms of the residuals is 3.6 m s^{-1}. The periodogram of the residuals shows a weak peak at 150 days that could be due to another companion. The rms of the residuals drops to 1.7 m s^{-1} when this second signal is adjusted. Since activity is still expected to have a few m s^{-1} amplitude jitter, we did not consider this additional companion as significant based on the present data set. It could rather be an activity artifact, with a semi-periodic signal at ∼times the rotational period.

3.4. HD 108341

The K star HD 108341was observed 24 times with HARPS over more than ten years, with individual RV errors of 1.9 m s^{-1} average. The star has a low activity index, and neither the bisector nor the CaII index varies with velocity. The RV variations of

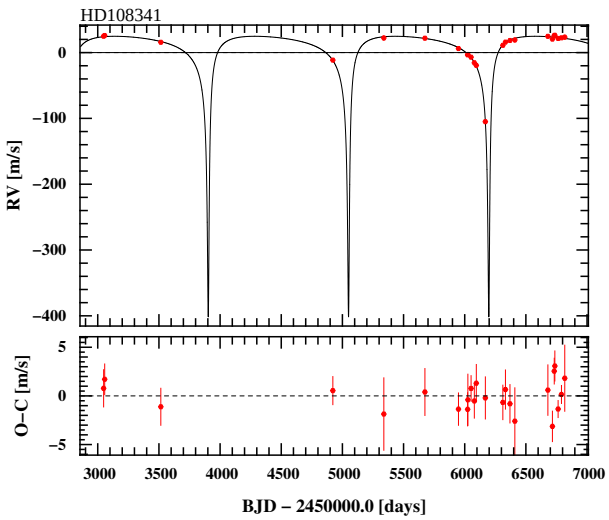

Fig. 6. Radial-velocity measurements of HD 108341 obtained with HARPS against time (*top*) and the residual to the best-fit model (*bottom*).

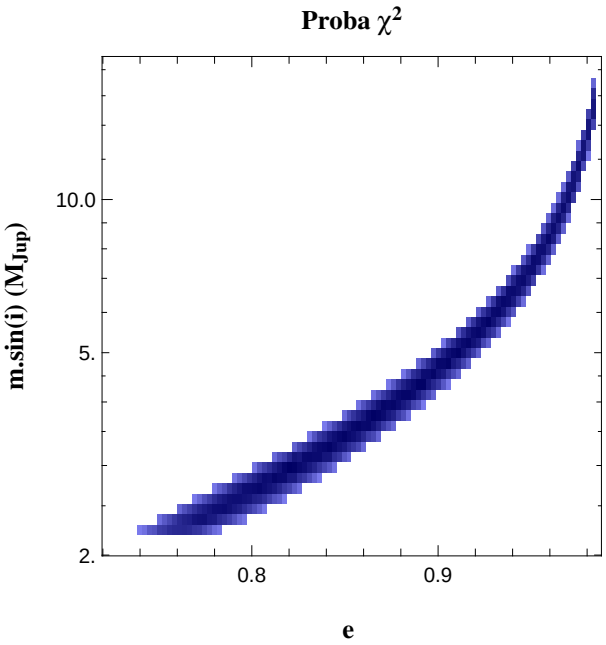

Fig. 7. χ^2 map of the companion mass and eccentricity obtained from the RV data set of HD 108341.

HD 108341 span from −110 m s^{-1} to +20 m s^{-1}, featuring the signature of a possible eccentric companion. When adjusted by a Keplerian orbit, the best-fit solution has a semi-amplitude of 144^{+311}_{-66} m s^{-1} and a period of 1129 days (Fig. 6). When this signal is removed, the rms of the residuals is 1.5 m s^{-1}, which is at the photon noise limit. Although the periastron passage is still undersampled, resulting in a large, asymmetric uncertainty in the final parameters (Table 2), we are confident that the detection of a giant planet in an eccentric orbit at about 2 AU semi-major axis is definite. The large uncertainty on the semi-amplitude is due to this incomplete periastron coverage, resulting in a two-peaked posterior distribution of most orbital parameters. The correlation between eccentricity and companion mass, as allowed by the data, is shown in Fig. 7. At this stage, the companion mass is only poorly constrained (2.3 to 6.9 $M_{\rm Jup}$ in the 68.3% confidence interval). Additional HARPS measurements, especially in August 2015 during next expected periastron passage, will decrease the error bars on the mass, period, and eccentricity.

3.5. HD 113538

We present here an update of the analysis of HARPS measurements of HD 113538, in which two planets were already reported in Moutou et al. (2011). We have now collected 75 HARPS measurements of HD 113538, spanning 3700 days, while there were only 29 (over 2268 days) in the previous study and much uncertainty remained on the parameters of these companions. The star is metal-poor and of late spectral type; the latter explains why $\log R'_{\rm HK}$ could not be estimated (nor the expected activity jitter), the stellar parameters were beyond reliable calibration boundaries. However, the behavior of the CaII S index as a function of time shows signs of activity and possible long-term cycling (Fig. 11). The chromospheric activity of the star currently increases after a minimum about four years earlier.

As in 2011, the current RV data set of HD 113538 is again better adjusted by the combination of two Keplerian curves. When adjusted with a first Keplerian, the best-fit corresponds to a period of 1870 days and a semi-amplitude of 24 m s^{-1}; the rms of the residuals is 7 m s^{-1}. The periodogram of the residuals shows a strong and well-defined peak at 660 days and another weaker peak at about 250 days. This latter peak – which lies close to the yearly alias of the former – disappears from the residuals when a two-Keplerian fit (including the 660 day signal) is applied. The rms of the residuals is 3.4 m s^{-1}after the two planet signatures are removed. The periodograms when one and two planet signals are removed are shown in Fig. 8 together with phase-folded RV series and RV against time plots. The final parameters of the planets are given in Table 3. Compared with the earlier solution proposed by Moutou et al. (2011), they are also affected by the update on the stellar mass (see Sect. 2).

Almost four additional years of continuous monitoring of this star have finally deeply changed the system solution since the first attempt by Moutou et al. (2011). The new parameters of the system are better constrained. However, with an increase in the chromospheric activity of the star, it is not clear whether the coming years will have optimal conditions to pursue observations on this target. The increasing level of activity may impact the tenuous signal detected from these planets and hamper an even better constraining of their parameters. We made the experiment of removing the last 20 data points, which correspond to the activity increase. It has the effect of reducing the longest period (to 1584 ± 30 days) and slightly changes the position of the second, lower-amplitude and shorter-period signal near 600 days. The final solution achieved on this data set therefore still depends on the specific data set used. With a span of the measurements so close to twice the period of the longest planet (3770-day span and 1820-day period) and a second maximum observed at JD ∼ 2 456 700, we are confident that our determination using the full data set is currently the most accurate. But another update in a few years would be profitable since there is room for improvement in the determination of the planetary and orbital parameters. However, stellar activity may be an issue as its level is currently increasing.

3.6. BD -114672

We have doubled the number of HARPS measurements of star BD -114672 since the first observation reported by Moutou et al. (2011) and updated the stellar mass (Sect. 2). The new data set spans 3271 days and is composed of

Table 3. Orbital and physical parameters for the two planets around HD 113538 presented in this paper.

Parameter			HD 113538 b	HD 113538 c
P	[days]		663.2 (–7.4, +8.4)	1818 (–22, +25)
T	[JD-2 454 000]		1500 (17)	2741 (31)
e			0.14 (0.08)	0.20 (0.04)
ω	[deg]		74 (–29, +37)	280 (16)
K	[m s^{-1}]		12.2 (1.1)	22.6 (0.8)
$a_1 \sin i$	[10^{-3} AU]		0.73 (0.06)	3.70 (0.13)
$m_2 \sin i$	[$M_{\rm Jup}$]		0.36 (0.04)	0.93 (0.06)
a	[AU]		1.24 (0.04)	2.44 (0.07)
γ	[km s^{-1}]	39.2 (0.6)		
$N_{\rm meas}$		75		
Span	[days]	3771		
σ (O–C)	[m s^{-1}]	3.5		
$\chi^2_{\rm red}$		3.4		

Notes. Median values are shown, and 1σ errors are given in parenthesis.

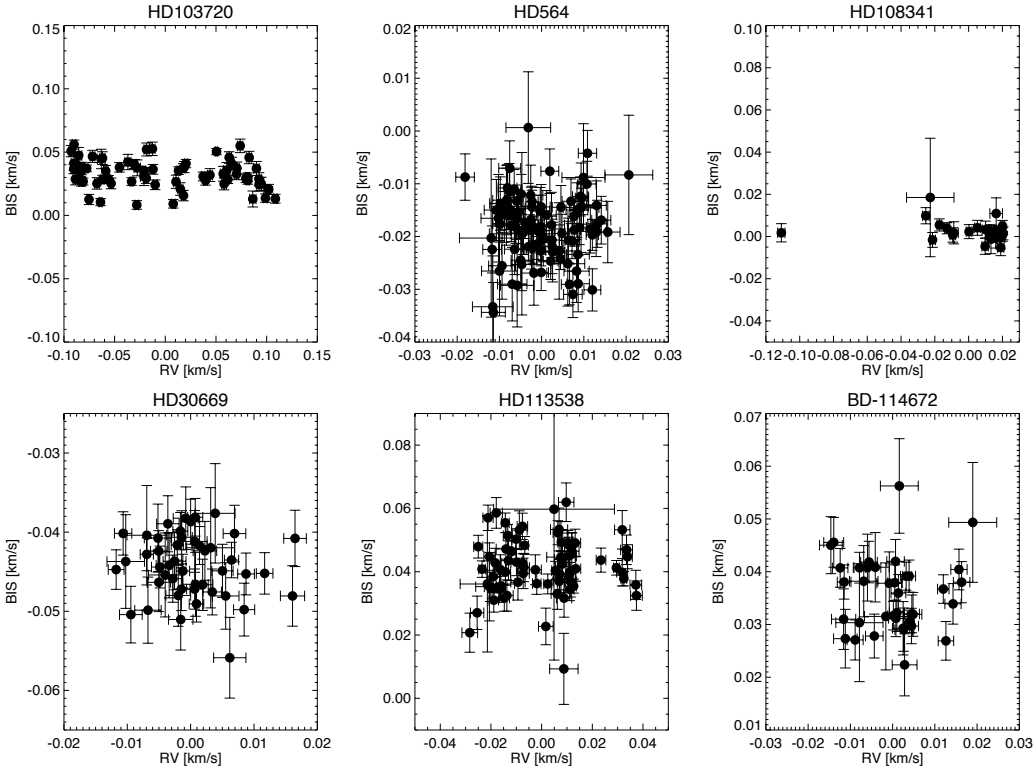

Fig. 10. Bisector versus radial velocity.

40 measurements, with an average uncertainty of 1.8 m s^{-1}. In the previous analysis, we had stayed conservative as the combined analysis of the activity and RV data was inconclusive. There was a non-negligible correlation between the cross-correlation function parameters and the CaII index, and the bisector was anticorrelated with the velocities. Since the time span of the observations was then also too short compared with the possible period and because activity potentially was a problem, we proposed conclusions of both a long-distant planet and a magnetic cycle.

With the increased data set, the impact of activity has dropped. As shown in Fig. 10, the anticorrelation between the bisector span and the radial velocity is not visible anymore. The evolution of the CaII S index with time (Fig. 11) is now constant. Finally, the correlation between this index and the FWHM of the cross-correlation function (as evoked in Moutou et al. 2011) is weaker, with a coefficient decreasing from 72% to 50%.

The planet scenario, in turn, has gained significance. The peak in the periodogram is more pronounced, and with two cycles just covered, the RV signal is better determined. A Keplerian fit gives a best solution characterized by a period of 1667 days, a circular orbit, and semi-amplitude 13 m s^{-1}, as shown in Fig. 9. The exact parameters and their errors after the MCMC analysis are given in Table 2. The rms of the residuals is 2.9 m s^{-1} when this signal is removed. The O–C residuals do show some pattern when plotted against the FWHM of the cross-correlation function, meaning that chromospheric activity is still present, but at a lower level that previously thought.

4. Discussion

RV Doppler signals due to planets are plagued by stellar activity (e.g., Saar et al. 1998; Desort et al. 2007; Boisse et al. 2009). Even searching for giant planets, this may remain the

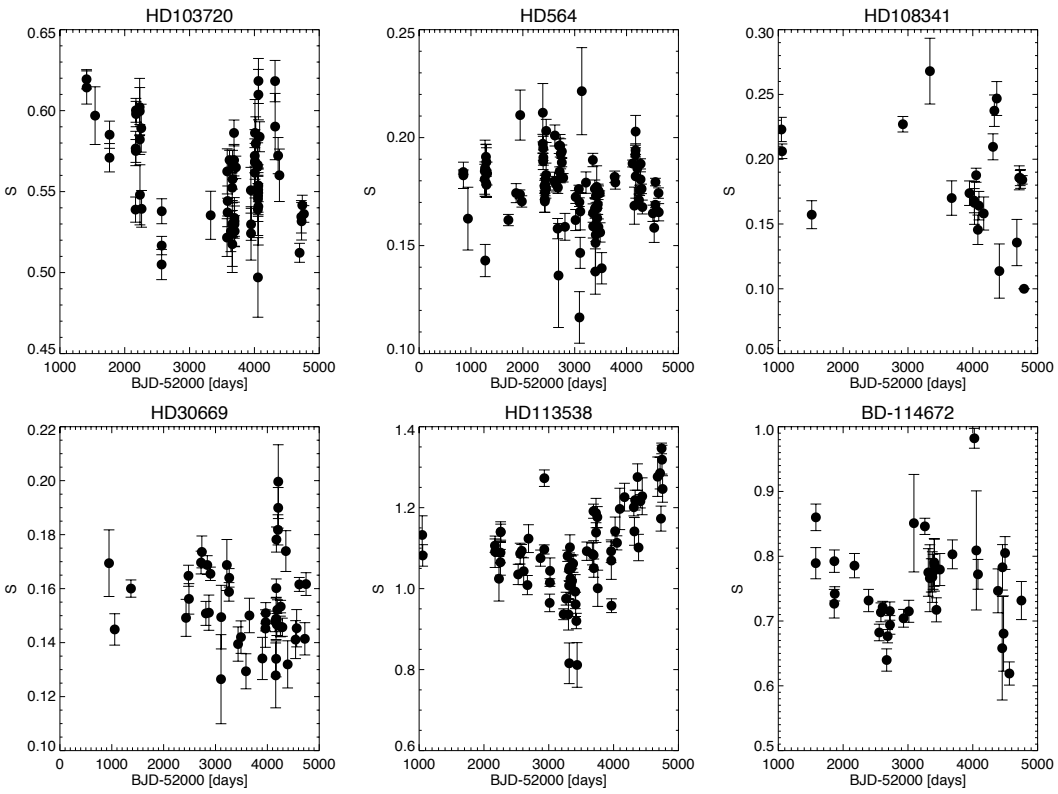

Fig. 11. Mount Wilson S activity index versus time.

main problem. Removing activity signatures (e.g., Dumusque et al. 2011; Haywood et al. 2014) is only possible when the highest precision is obtained on the RV measurement and on other parameters of the cross-correlation function and when the highest S/N spectra are collected, since the CaII emission is measured on the bluest part of the spectra, which receive the lowest photon count on these relatively cool objects. If activity correction is expected to improve the extraction of the planet signal, activity indicators need to be measured with the highest possible precision. In the sample of measurements discussed in this article, there are at least three cases where stellar activity plays a role: i) the identification of the hot-Jupiter planetary signal of HD 103720; ii) the anterior misinterpretation of the signal of BD -114672; and iii) the power distribution in the periodogram of the CaII measurements for HD 564. In the first case, strong jitter masked out the main planetary signal; without any clear correlation between the bisector span and the radial velocity and with a small $\log R'_{\rm HK}$, it was difficult to assess the real impact of the stellar activity on the RV signal. Even for a K = 89 m s^{-1} semi-amplitude Doppler wobble, the star required extensive follow-up over several years. The complexity of stellar surfaces in some stars prevents a clear BIS-RV relation from appearing, as in Boisse et al. (2009), Melo et al. (2007), and an auto-correction of the cross-correlation function (i.e., removal of the BIS-RV slope) is impossible or would just add random noise. In the second case, the RV time series of BD -114672 showed a significant correlation with the CaII index and the bisector span based on the first five years of measurements, and these correlations are not significant anymore after five additional years of observations. In the last case, there is a peak near the orbital period in the Lomb-Scargle periodogram of the CaII measurements of HD 564, although its main properties show a quiet solar-like star. Dispersion in the activity indicators of HD 564 is also seen, and the signal amplitudes are small, which complicates the global interpretation. In all three cases, we are confident about the planetary signals as interpreted in Sect. 3, but future measurements could induce modifications of these conclusions.

The long-term evolution of all these activity parameters and their dependencies on the radial velocity are thus difficult to understand, especially with a limited amount of observing time per target in a volume-limited survey, where the highest precision or the densest observing cadence cannot be achieved.

In the case of hot Jupiters, it has been expected that massive planets close to the star surface may induce extra photospheric activity (Shkolnik et al. 2003). The host star of the hot Jupiter HD 130720 b is an active star, and we searched for the potential signature of activity of such a star in our measurements. With a stellar rotation period of about 10 days, and thus at a synodic period of ~8 days, no visible trend is visible in our data, however, the S/N of the individual CaII measurements is much lower than in previous similar attempts (Shkolnik et al. 2008; Fares et al. 2012). As expected, we found no period in the CaII index that could indicate induced activity. In addition, the *Galex* flux of HD 103720 in the far-UV and near-UV domain was compared with the general population of stars with hot Jupiters and distant Jupiters, as discussed in Shkolnik (2013): the UV flux values are similar to those of other planet hosts, and this new case fits well with the conclusions of this study (i.e., no clear impact on the UV stellar flux from the close-in planet).

The long-period giant planets constitute the important population from which the overlap with the direct imaging method is possible. Of the new planets presented in this work, the system around HD 113538 is the most promising regarding angular separation, as a planet-star separation of 0.08 and 0.15 arcsec is expected for the inner and outer planets. This corresponds to 1.5 and 3 times the resolution in the J band and could be within reach of the new-generation extreme adaptive-optics instruments such as ESO/SPHERE and Gemini/GPI. However, the system

is evolved (age of several Gyr), and both these planets have a minimum mass smaller than the Jupiter mass, and their intrinsic luminosity is extremely faint (absolute magnitude 35 or more) while the reflected luminosity is damped by a too large orbital distance.

The new planets have been added to the known population of giant exoplanets (filled circles in Fig. 1). HD 103720 b piles up with other hot Jupiters of mass lower than Jupiter's, with a period slightly longer than other, more massive giant planets; it is a close twin of υ And b, whose host star is significantly more massive, however (1.27 $M_{\odot}$ instead of 0.79 $M_{\odot}$). All other planets are giant and distant planets with minimum masses between those of Saturn and Jupiter and semi-major axes between 1 and 3 AU, hence in populated areas of the mass and orbital distance parameter space, as predicted by the core-accretion formation model (Mordasini et al. 2009; Ida et al. 2013; Benz et al. 2014, and references therein).

From the new sample of giant exoplanets reported in this work, only HD 564 b lies in the habitable zone (HZ) of its parent star. The planet around HD 103720 is too hot and planets around HD 30669, HD 108341, HD 113538, and BD -114672 are too cold according to the HZ definition of Kasting et al. (1993). HD 564 b has a mass similar to that of Saturn; if it were, as Saturn, orbited by a set of moons, especially large ones like Titan, life as we know it could probably emerge and develop on these moons (Williams et al. 1997). Detection of such a moon with the current methods and instruments is extremely challenging, however, as outlined by Kipping (2014).

Finally, the systems characterized here would strongly benefit from additional observations. As discussed above, such planets in a period range longer than three years with a semi-amplitude RV signal of a few tens of m s^{-1} are numerous, and the planet parameters may vary with time when the full period of the orbit is not covered, the stellar activity is somewhat high, or/and the observational S/N is too low for a precise measurement of the activity indicators. A long observing sequence allows either to average the activity signal down, to select parts of the sequence that are less affected, or to reveal additional companions that create the RV jitter. Long-term observational efforts using ELODIE/SOPHIE (Boisse et al. 2012), Lick/Keck-HIRES (Fischer et al. 2014), CORALIE (Marmier et al. 2013), and HARPS (Lo Curto et al. 2010; Mayor et al. 2011) should thus be followed-up as long as the hardware and facilities exist and perform at a precision level of a few m s^{-1}.

Note added in proof. The light curve of HD 103720 has been obtained with K2 in summer 2014 in long cadence (http://archive.stsci.edu/k2/). After analysis of pixel data, the rms of the light curve is 246 ppm. No transit is found at the expected ephemeris and depth (Barros, Demangeon, Santerne, Deleuil, priv. comm.). Searching for transits of HD 103720 b is not required anymore.

Acknowledgements. N.C.S. and S.G.S. acknowledge the support from Fundação para a Ciência e a Tecnologia (FCT, Portugal) through FEDER funds in program COMPETE, as well as through national funds, in the form of grants reference RECI/FIS-AST/0176/2012 (FCOMP-01-0124-FEDER-027493) and RECI/FIS-AST/0163/2012 (FCOMP-01-0124-FEDER-027492). We also acknowledge the support from the European Research Council/European Community under the FP7 through Starting Grant agreement number 239953. N.C.S. was supported by FCT through the Investigador FCT contract reference IF/00169/2012 and POPH/FSE (EC) by FEDER funding through the program "Programa Operacional de Factores de Competitividade – COMPETE". S.G.S. was supported by FCT through the grant with the reference SFRH/BPD/47611/2008. We are grateful to the ESO staff for their support during observations.

References

Allard, F., Homeier, D., Freytag, B., et al. 2013, Mem. Soc. Astron. It. Suppl., 24, 128
Baranne, A., Queloz, D., Mayor, M., et al. 1996, A&AS, 119, 373
Benz, W., Ida, S., Alibert, Y., Lin, D. N. C., & Mordasini, C. 2014, in Protostars and Planets VI (University of Arizona Press), eds. H. Beuther, R. Klessen, C. Dullemond, & Th. Henning, 691
Beuzit, J.-L., Feldt, M., Dohlen, K., et al. 2008, in SPIE Conf. Ser., 7014
Boisse, I., Moutou, C., Vidal-Madjar, A., et al. 2009, A&A, 495, 959
Boisse, I., Bouchy, F., Hébrard, G., et al. 2011, A&A, 528, A4
Boisse, I., Pepe, F., Perrier, C., et al. 2012, A&A, 545, A55
Chen, Y., Girardi, L., Bressan, A., et al. 2014, MNRAS, 444, 2525
da Silva, L., Girardi, L., Pasquini, L., et al. 2006, A&A, 458, 609
Desort, M., Lagrange, A.-M., Galland, F., Udry, S., & Mayor, M. 2007, A&A, 473, 983
Dumusque, X., Lovis, C., Ségransan, D., et al. 2011, A&A, 535, A55
Fares, R., Donati, J.-F., Moutou, C., et al. 2012, MNRAS, 423, 1006
Fischer, D. A., Marcy, G. W., & Spronck, J. F. P. 2014, ApJS, 210, 5
Haywood, R. D., Collier Cameron, A., Queloz, D., et al. 2014, MNRAS, 443, 2517
Ida, S., Lin, D. N. C., & Nagasawa, M. 2013, ApJ, 775, 42
Kasting, J. F., Whitmire, D. P., & Reynolds, R. T. 1993, Icarus, 101, 108
Kipping, D. M. 2014, Proc. for the Frank N. Bash Symp. 2013: New Horizons in Astronomy, held October 6–8, 2013 in Austin, TX, submitted [arXiv:1405.1455]
Lo Curto, G., Mayor, M., Benz, W., et al. 2010, A&A, 512, A48
Lovis, C., Dumusque, X., Santos, N. C., et al. 2011, unpublished [arXiv:1107.5325]
Macintosh, B. A., Graham, J. R., Palmer, D. W., et al. 2008, in SPIE Conf. Ser., 7015
Mamajek, E. E., & Hillenbrand, L. A. 2008, ApJ, 687, 1264
Marmier, M., Ségransan, D., Udry, S., et al. 2013, A&A, 551, A90
Mayor, M., Pepe, F., Queloz, D., et al. 2003, The Messenger, 114, 20
Mayor, M., Marmier, M., Lovis, C., et al. 2011, A&A, submitted [arXiv:1109.2497]
Melo, C., Santos, N. C., Gieren, W., et al. 2007, A&A, 467, 721
Mordasini, C., Alibert, Y., Benz, W., & Naef, D. 2009, A&A, 501, 1161
Moutou, C., Mayor, M., Lo Curto, G., et al. 2011, A&A, 527, A63
Noyes, R. W., Hartmann, L. W., Baliunas, S. L., Duncan, D. K., & Vaughan, A. H. 1984, ApJ, 279, 763
Queloz, D., Henry, G. W., Sivan, J. P., et al. 2001, A&A, 379, 279
Saar, S. H., Butler, R. P., & Marcy, G. W. 1998, ApJ, 498, L153
Santos, N. C., Mayor, M., Naef, D., et al. 2000, A&A, 361, 265
Santos, N. C., Gomes da Silva, J., Lovis, C., & Melo, C. 2010, A&A, 511, A54
Ségransan, D., Mayor, M., Udry, S., et al. 2011, A&A, 535, A54
Shkolnik, E. L. 2013, ApJ, 766, 9
Shkolnik, E., Walker, G. A. H., & Bohlender, D. A. 2003, ApJ, 597, 1092
Shkolnik, E., Bohlender, D. A., Walker, G. A. H., & Collier Cameron, A. 2008, ApJ, 676, 628
Sousa, S. G., Santos, N. C., Israelian, G., Mayor, M., & Monteiro, M. J. P. F. G. 2007, A&A, 469, 783
Sousa, S. G., Santos, N. C., Mayor, M., et al. 2008, A&A, 487, 373
Sousa, S. G., Santos, N. C., Israelian, G., Mayor, M., & Udry, S. 2011, A&A, 533, A141
Spiegel, D. S., & Burrows, A. 2012, ApJ, 745, 174
van Leeuwen, F. 2007, A&A, 474, 653
Watson, C., Henden, A. A., & Price, A. 2014, VizieR Online Data Catalog, B/vsx
Williams, D. M., Kasting, J. F., & Wade, R. A. 1997, Nature, 385, 234
Wright, J. T. 2005, PASP, 117, 657

Pages 10 to 14 are available in the electronic edition of the journal at http://www.aanda.org

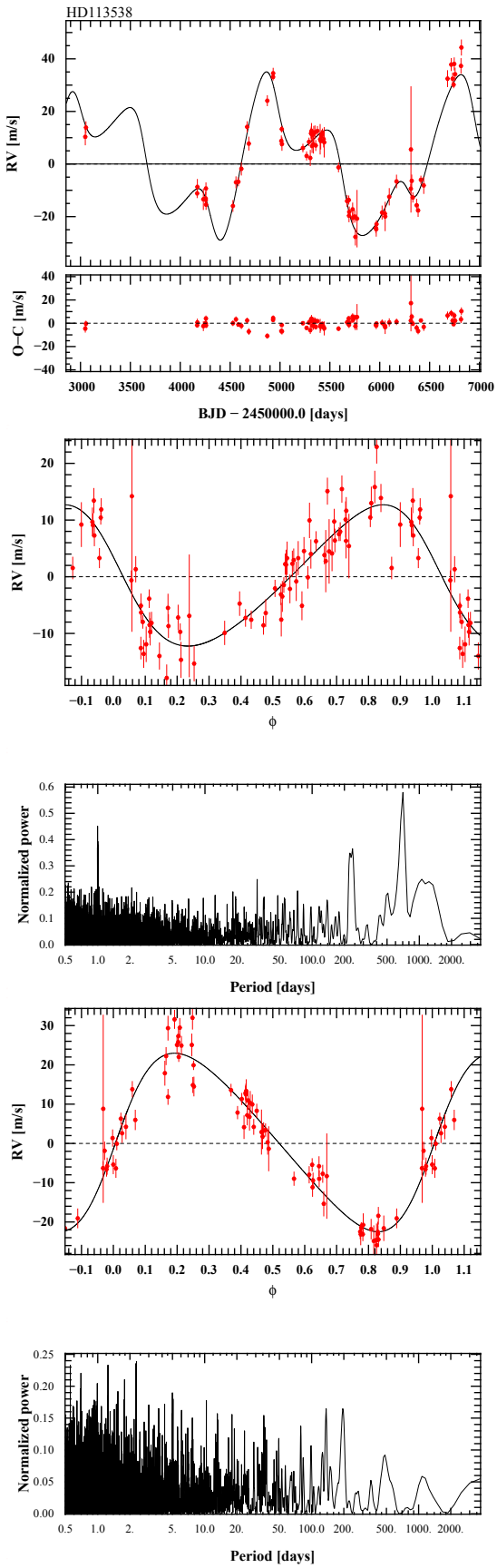

Fig. 8. Radial-velocity measurements of HD 113538 obtained with HARPS against time (*top*) and versus phase for both planets (*second line*: 660-day period planet; *fourth line*: 1800-day period planet). The periodograms of the residuals after 1 (2) planet(s) are removed are shown in the *third* and *fifth* lines.

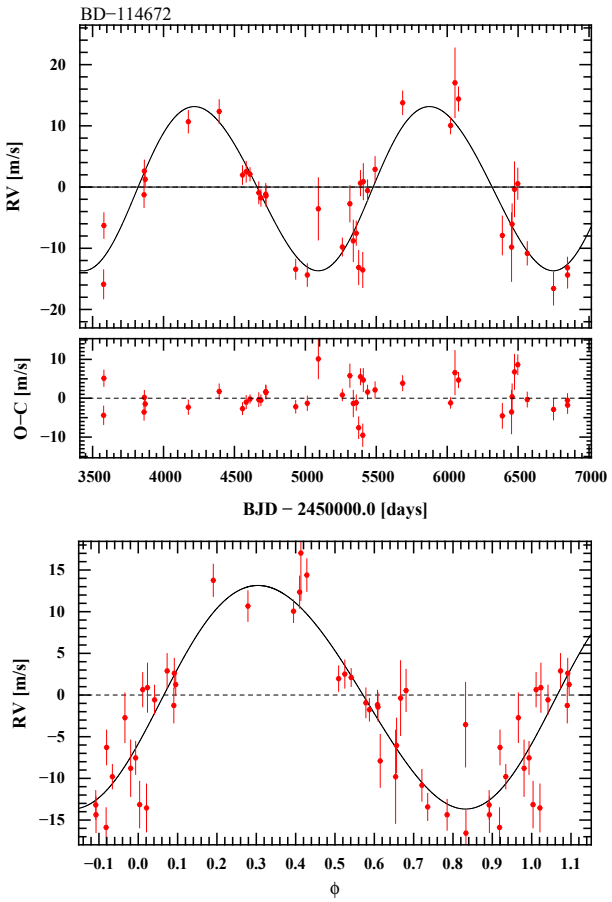

Fig. 9. Radial-velocity measurements of BD -114672 obtained with HARPS against time (*top*) and phase (*bottom*).

Table 4. Radial-velocity measurements obtained with HARPS of HD 103720.

JD-2 400 000.	RV [km s^{-1}]	σ_{RV} [km s^{-1}]	BIS [km s^{-1}]	S_{MW}	S/N
53 410.725537	–6.42457	0.00158	0.01744	0.622044	53.40
53 410.750724	–6.42760	0.00158	0.02400	0.616814	53.30
53 412.732968	–6.61754	0.00178	0.05596	0.614279	49.10
53 542.554647	–6.43757	0.00276	0.03710	0.596911	33.20
53 764.875570	–6.49020	0.00173	0.03076	0.570907	47.70
53 765.779982	–6.42867	0.00166	0.01368	0.585120	50.00
54 166.758756	–6.46572	0.00159	0.02844	0.538893	51.20
54 168.742727	–6.60277	0.00202	0.01259	0.576631	41.80
54 170.746496	–6.44605	0.00152	0.02771	0.575096	53.70
54 172.764332	–6.56071	0.00152	0.02676	0.600196	54.20
54 174.726235	–6.50707	0.00163	0.04095	0.597889	50.50
54 229.652114	–6.46689	0.00307	0.03563	0.602207	30.00
54 231.664769	–6.54597	0.00256	0.05207	0.599676	34.80
54 232.559019	–6.61496	0.00190	0.04002	0.582196	43.80
54 234.598066	–6.44116	0.00316	0.01298	0.548020	29.30
54 254.493249	–6.54019	0.00265	0.05261	0.589170	33.60
54 259.550772	–6.58628	0.00221	0.03511	0.539361	38.20
54 568.647269	–6.53749	0.00191	0.02419	0.504989	43.10
54 569.640520	–6.60856	0.00138	0.02683	0.516682	56.80
54 570.648595	–6.55564	0.00171	0.00828	0.537879	47.00
55 325.571974	–6.58948	0.00253	0.04524	0.535369	36.20
55 577.838644	–6.50951	0.00207	0.01567	0.521618	42.90
55 580.784534	–6.59489	0.00227	0.02530	0.562490	40.80
55 586.829408	–6.51970	0.00167	0.00917	0.537119	52.10
55 587.842698	–6.41890	0.00173	0.01321	0.544208	50.70
55 616.703495	–6.54845	0.00129	0.03539	0.569496	66.90
55 637.714149	–6.46446	0.00226	0.04577	0.525493	39.70
55 657.704287	–6.55822	0.00175	0.04059	0.552351	50.00
55 658.726448	–6.61764	0.00276	0.04118	0.517552	34.30
55 659.606019	–6.55516	0.00316	0.03756	0.524144	30.70
55 660.662655	–6.44801	0.00167	0.02931	0.530118	51.70
55 662.628820	–6.58349	0.00136	0.02880	0.557618	61.70
55 663.657096	–6.61054	0.00175	0.02668	0.566528	49.80
55 685.596119	–6.58948	0.00165	0.02840	0.586229	52.50
55 686.566390	–6.61100	0.00191	0.03462	0.569396	46.10
55 690.670990	–6.61621	0.00226	0.02865	0.533763	40.10
55 692.639087	–6.44475	0.00244	0.04575	0.529892	37.40
55 693.560870	–6.48774	0.00184	0.02761	0.531775	47.40
55 695.513106	–6.61786	0.00184	0.03668	0.525540	47.70
55 714.590148	–6.51440	0.00151	0.03540	0.564957	56.20
55 945.872673	–6.62038	0.00225	0.05078	0.550842	41.20
55 947.857270	–6.45361	0.00267	0.05497	0.524203	35.00
55 948.841893	–6.50988	0.00176	0.03739	0.529801	50.10
56 005.704890	–6.57270	0.00185	0.03797	0.572106	48.10
56 006.681664	–6.45683	0.00241	0.03736	0.561616	38.80
56 007.675207	–6.47036	0.00291	0.03292	0.568068	33.30
56 008.688587	–6.56441	0.00302	0.04218	0.586245	32.20
56 009.754245	–6.61010	0.00187	0.03584	0.568689	48.10
56 020.644924	–6.43282	0.00260	0.02495	0.579611	35.90
56 051.689679	–6.51262	0.00248	0.02083	0.566476	37.90
56 052.530097	–6.43495	0.00266	0.02445	0.565486	35.30
56 053.501755	–6.48342	0.00253	0.03189	0.538947	37.40
56 054.588635	–6.59068	0.00386	0.04458	0.497023	26.20
56 055.573461	–6.59932	0.00242	0.04659	0.545490	37.80
56 056.626337	–6.45720	0.00222	0.03269	0.547406	40.70
56 057.485811	–6.42548	0.00198	0.02057	0.549510	46.20
56 058.524010	–6.51691	0.00261	0.02659	0.551157	35.80
56 059.607215	–6.60978	0.00181	0.03832	0.553824	49.40
56 060.575567	–6.54854	0.00355	0.03068	0.540806	28.20
56 061.589262	–6.43499	0.00256	0.02865	0.609882	36.30
56 062.561883	–6.46946	0.00236	0.02492	0.618299	38.70
56 080.511699	–6.44618	0.00170	0.03021	0.583868	52.60
56 318.829398	–6.58097	0.00212	0.02528	0.618238	44.70
56 319.790147	–6.61293	0.00312	0.04747	0.590154	32.00
56 365.732344	–6.54633	0.00203	0.02942	0.572228	44.40
56 385.740518	–6.46192	0.00253	0.04090	0.560083	38.10
56 696.877943	–6.60508	0.00130	0.03711	0.512218	65.50
56 723.694284	–6.53963	0.00192	0.03643	0.534451	46.30
56 727.758738	–6.50879	0.00220	0.03820	0.531676	40.80
56 738.742879	–6.59142	0.00143	0.01051	0.541591	59.70
56 763.650168	–6.47696	0.00123	0.05046	0.536203	67.70

Notes. S/N gives the signal-to-noise value per pixel at 550 nm.

Table 5. Radial-velocity measurements obtained with HARPS of HD 564.

JD-2 400 000.	RV [km s^{-1}]	σ_{RV} [km s^{-1}]	BIS [km s^{-1}]	S_{MW}	S/N
52 851.876768	11.46301	0.00116	–0.02048	0.184060	126.30
52 853.869168	11.46523	0.00284	–0.02295	0.182541	43.10
52 941.607800	11.48328	0.00566	–0.00832	0.162482	23.40
53 264.713004	11.44450	0.00220	–0.00873	0.180716	53.50
53 266.724775	11.45493	0.00197	–0.01473	0.184430	55.80
53 271.732825	11.45242	0.00414	–0.01653	0.185826	30.90
53 274.738912	11.45120	0.00284	–0.03438	0.143082	41.00
53 288.679402	11.45507	0.00259	–0.00705	0.191112	40.70
53 291.680278	11.45266	0.00426	–0.02654	0.184789	28.20
53 294.677291	11.46005	0.00286	–0.01219	0.178598	35.10
53 296.692360	11.45192	0.00290	–0.01498	0.188696	36.10
53 298.715144	11.45380	0.00275	–0.01561	0.178162	36.40
53 310.662439	11.46287	0.00227	–0.02000	0.183368	48.60
53 721.566682	11.45269	0.00160	–0.01758	0.161832	61.40
53 870.933543	11.45767	0.00226	–0.02449	0.174302	44.60
53 944.861248	11.47027	0.00142	–0.01619	0.173747	68.70
53 948.860547	11.46677	0.00456	–0.02274	0.210435	25.10
53 980.770152	11.46982	0.00166	–0.02086	0.170453	58.70
54 384.726844	11.46376	0.00231	–0.01591	0.197163	44.10
54 385.634255	11.45947	0.00529	0.00065	0.211525	22.50
54 391.641142	11.47579	0.00223	–0.01759	0.188990	43.90
54 393.663465	11.47829	0.00291	–0.01915	0.195049	34.90
54 395.681422	11.47337	0.00216	–0.01004	0.190786	45.30
54 420.585952	11.47179	0.00185	–0.01240	0.177270	53.70
54 423.589368	11.47090	0.00298	–0.02655	0.171492	35.30
54 424.516514	11.47099	0.00259	–0.01498	0.170450	39.70
54 426.542184	11.46958	0.00212	–0.01332	0.174664	46.10
54 429.520725	11.47675	0.00226	–0.01690	0.178376	44.80
54 430.643552	11.47348	0.00217	–0.00422	0.177047	46.70
54 437.595286	11.47218	0.00157	–0.01269	0.180847	62.90
54 446.594441	11.47554	0.00231	–0.01918	0.176365	44.60
54 448.541103	11.47121	0.00272	–0.02339	0.182717	38.30
54 450.542773	11.47128	0.00266	–0.02895	0.203111	38.90
54 609.908159	11.46230	0.00223	–0.01515	0.179853	45.70
54 617.933002	11.45791	0.00249	–0.02531	0.200989	41.60
54 637.902968	11.45669	0.00200	–0.01659	0.178432	50.80
54 670.781602	11.45625	0.00240	–0.02241	0.157861	43.20
54 675.855760	11.45714	0.00179	–0.01883	0.176921	54.90
54 687.930372	11.45068	0.00750	–0.02029	0.136157	17.90
54 698.797546	11.46021	0.00213	–0.02191	0.196208	46.40
54 709.844063	11.45673	0.00152	–0.01328	0.184255	65.60
54 719.755513	11.45500	0.00266	–0.01147	0.196230	39.30
54 722.825809	11.45542	0.00153	–0.01793	0.181264	64.60
54 730.740618	11.45325	0.00318	–0.02554	0.192506	34.30
54 751.725433	11.45327	0.00144	–0.01583	0.188489	68.70
54 752.622288	11.45613	0.00188	–0.01105	0.193610	52.30
54 778.571503	11.46036	0.00145	–0.01336	0.181394	67.30
54 812.570368	11.46080	0.00304	–0.02692	0.158688	34.80
55 016.915860	11.46173	0.00271	–0.01891	0.161838	36.90
55 018.861671	11.46745	0.00183	–0.01943	0.172494	54.70
55 079.807536	11.45950	0.00136	–0.02195	0.176188	72.30
55 090.789049	11.46052	0.00146	–0.02214	0.170126	67.90
55 091.643857	11.45106	0.00481	–0.03331	0.116738	24.40
55 105.694107	11.45433	0.00328	–0.01311	0.146626	33.30
55 107.683151	11.45683	0.00394	–0.02926	0.165819	28.60
55 136.581223	11.45795	0.00770	–0.01947	0.221511	17.20
55 217.538712	11.45284	0.00253	–0.01375	0.179174	41.80
55 349.887745	11.46477	0.00175	–0.02466	0.189634	59.30
55 352.952710	11.46457	0.00211	–0.00762	0.165068	50.60
55 355.889795	11.46512	0.00258	–0.02188	0.158900	41.50
55 388.885020	11.46253	0.00212	–0.01438	0.176285	49.20
55 391.894404	11.47003	0.00220	–0.03096	0.167251	48.90
55 397.867729	11.47196	0.00424	–0.01453	0.137993	27.60
55 401.791292	11.47254	0.00509	–0.00882	0.151250	23.80
55 404.844242	11.46508	0.00227	–0.02066	0.167329	45.50
55 405.930310	11.47157	0.00164	–0.01824	0.154994	64.70
55 409.891367	11.47203	0.00171	–0.01425	0.173069	62.70
55 424.709058	11.46882	0.00402	–0.02515	0.177195	29.00
55 433.869077	11.47036	0.00154	–0.01876	0.167255	68.90
55 434.713976	11.47563	0.00232	–0.01409	0.162711	46.10
55 445.650274	11.47416	0.00228	–0.01857	0.169120	47.10
55 453.679814	11.46923	0.00194	–0.02907	0.174891	54.10
55 457.614894	11.47464	0.00199	–0.03012	0.158611	53.00
55 460.786864	11.47464	0.00148	–0.01968	0.175336	70.00
55 482.664228	11.46709	0.00102	–0.02422	0.174177	101.00
55 490.774792	11.46720	0.00205	–0.01445	0.156100	52.70
55 520.603912	11.46248	0.00336	–0.01886	0.139505	33.00
55 770.909913	11.46034	0.00159	–0.01441	0.181841	65.70
55 782.894474	11.45780	0.00187	–0.01196	0.179220	54.60
56 115.896670	11.45713	0.00116	–0.01535	0.188004	90.80
56 150.766066	11.45566	0.00349	–0.02903	0.168490	33.20
56 169.766216	11.45456	0.00223	–0.01079	0.192058	48.30
56 173.851140	11.45544	0.00170	–0.01593	0.194119	63.80
56 174.794849	11.46014	0.00311	–0.01688	0.202797	36.80
56 175.913555	11.45429	0.00365	–0.01435	0.182058	32.90
56 207.734956	11.45833	0.00217	–0.01906	0.185766	49.80
56 239.619268	11.45269	0.00170	–0.01765	0.171106	62.70
56 253.606856	11.45868	0.00153	–0.01731	0.175562	71.10
56 269.598885	11.46143	0.00191	–0.02148	0.180665	56.90
56 271.533034	11.45986	0.00142	–0.01874	0.187842	78.80
56 289.545712	11.46245	0.00135	–0.01809	0.176270	80.50
56 304.523400	11.46253	0.00172	–0.02680	0.167858	64.70
56 506.912689	11.46897	0.00212	–0.02075	0.164968	51.20
56 532.870914	11.46497	0.00309	–0.01780	0.158232	37.20
56 555.807983	11.46251	0.00108	–0.02263	0.168914	97.40
56 556.866358	11.46072	0.00124	–0.01860	0.179422	85.30
56 615.616037	11.45646	0.00154	–0.01822	0.174320	69.30
56 620.518959	11.45092	0.00223	–0.02245	0.165451	48.00

Notes. S/N gives the signal-to-noise value per pixel at 550 nm.

Table 6. Radial-velocity measurements obtained with HARPS of HD 30669.

JD-2 400 000.	RV [km s^{-1}]	σ_{RV} [km s^{-1}]	BIS [km s^{-1}]	S_{MW}	S/N
52 946.812523	65.86486	0.00296	–0.04371	0.169431	31.20
53 056.566167	65.87576	0.00195	–0.04117	0.144889	45.50
53 369.720161	65.87603	0.00116	–0.04906	0.160031	65.80
54 431.697383	65.86837	0.00209	–0.04986	0.149176	38.10
54 478.695858	65.86445	0.00137	–0.04016	0.164764	56.90
54 487.585050	65.86567	0.00179	–0.05042	0.156202	44.00
54 720.903534	65.87229	0.00148	–0.04588	0.169663	50.90
54 736.855063	65.87009	0.00185	–0.04634	0.173602	41.90
54 814.693440	65.87700	0.00162	–0.04665	0.150827	46.90
54 841.635439	65.87511	0.00142	–0.03868	0.168755	52.20
54 872.604317	65.87586	0.00202	–0.04659	0.151099	39.90
54 902.527097	65.87319	0.00133	–0.04828	0.165943	57.30
54 902.533138	65.87281	0.00135	–0.03476	0.165018	56.70
55 105.808888	65.87827	0.00380	–0.04197	0.126462	24.00
55 109.822612	65.87898	0.00314	–0.03762	0.149445	27.20
55 218.690341	65.88129	0.00255	–0.05587	0.168758	33.80
55 260.550527	65.88385	0.00132	–0.04528	0.158792	58.90
55 264.532568	65.88679	0.00131	–0.04521	0.164005	59.20
55 434.908336	65.89159	0.00179	–0.04079	0.139469	45.20
55 490.873740	65.88203	0.00179	–0.04018	0.142034	44.10
55 587.538203	65.89119	0.00191	–0.04806	0.129387	43.20
55 653.511919	65.88355	0.00167	–0.04979	0.150054	50.50
55 903.735078	65.88064	0.00210	–0.04806	0.134130	39.80
55 962.518684	65.87736	0.00186	–0.04236	0.145218	44.80
55 966.562222	65.87388	0.00106	–0.04491	0.147531	77.80
55 968.629501	65.87349	0.00118	–0.03987	0.150913	70.20
56 149.914280	65.86335	0.00125	–0.04473	0.147855	63.80
56 160.905614	65.87109	0.00265	–0.04541	0.127865	33.50
56 167.891515	65.87172	0.00206	–0.04419	0.148821	40.30
56 168.878684	65.87151	0.00177	–0.03894	0.133997	46.60
56 171.855514	65.87650	0.00120	–0.04169	0.160186	67.80
56 173.912158	65.87852	0.00145	–0.04756	0.178192	56.20
56 181.837185	65.87365	0.00135	–0.04721	0.146710	60.10
56 191.919832	65.87574	0.00127	–0.04719	0.152157	65.30
56 204.832233	65.87369	0.00167	–0.04065	0.181777	49.00
56 208.878254	65.86995	0.00215	–0.04075	0.189935	38.50
56 209.872861	65.86819	0.00315	–0.04039	0.199631	29.00
56 251.698978	65.87025	0.00132	–0.04441	0.145983	63.90
56 256.788837	65.86819	0.00104	–0.04280	0.153352	82.90
56 289.697046	65.87007	0.00129	–0.04239	0.145702	62.30
56 356.527585	65.87257	0.00182	–0.04367	0.173913	48.00
56 391.492430	65.87434	0.00198	–0.03824	0.131935	45.10
56 543.870683	65.87354	0.00193	–0.05104	0.141112	43.90
56 564.828467	65.87315	0.00194	–0.04800	0.145339	43.30
56 615.788648	65.88156	0.00111	–0.04352	0.161555	71.40
56 722.552843	65.88013	0.00168	–0.04489	0.141415	49.60
56 745.477862	65.87729	0.00175	–0.03852	0.164149	49.10
56 745.481647	65.87466	0.00157	–0.03779	0.159891	53.60

Notes. S/N gives the signal-to-noise value per pixel at 550 nm.

Table 7. Radial-velocity measurements obtained with HARPS of HD 108341.

JD-2 400 000.	RV [km s^{-1}]	σ_{RV} [km s^{-1}]	BIS [km s^{-1}]	S_{MW}	S/N
53 047.806558	56.73236	0.00191	–0.00523	0.222966	46.40
53 056.826970	56.73343	0.00158	0.00088	0.206144	56.00
53 515.599740	56.72315	0.00190	–0.00463	0.157178	41.30
54 921.798313	56.69606	0.00144	0.00549	0.226998	51.40
55 338.656931	56.72967	0.00372	0.01091	0.267985	25.00
55 674.563476	56.72937	0.00241	–0.00064	0.170013	34.00
55 948.863549	56.71362	0.00166	0.00232	0.173786	48.00
56 023.742177	56.70398	0.00169	0.00073	0.168008	47.10
56 025.688336	56.70462	0.00263	0.00176	0.166300	32.40
56 051.736647	56.70056	0.00130	0.00392	0.187639	58.60
56 078.570007	56.69199	0.00175	–0.00161	0.145563	47.20
56 094.601475	56.68802	0.00192	0.00986	0.164142	42.90
56 168.472537	56.60249	0.00216	0.00177	0.158093	39.20
56 311.801063	56.71854	0.00177	0.00414	0.209571	47.10
56 332.784952	56.72480	0.00390	0.01071	0.205499	23.80
56 332.806377	56.72290	0.00232	0.00074	0.247088	36.30
56 369.746228	56.72588	0.00197	0.00129	0.246852	43.30
56 409.658101	56.72661	0.00343	–0.00126	0.113681	26.60
56 679.870605	56.73221	0.00260	–0.00068	0.135687	33.50
56 716.862191	56.72798	0.00157	0.00195	0.185636	51.40
56 731.662512	56.73342	0.00132	0.00499	0.185475	60.40
56 736.840769	56.73386	0.00154	0.00150	0.184786	51.70
56 763.585806	56.72894	0.00087	0.00267	0.184067	88.30

Notes. S/N gives the signal-to-noise value per pixel at 550 nm.

Table 8. Radial-velocity measurements obtained with HARPS of HD 113538.

JD-2 400 000.	RV [km s^{-1}]	σ_{RV} [km s^{-1}]	BIS [km s^{-1}]	S_{MW}	S/N
53 047.881823	39.23173	0.00305	0.06196	1.132572	35.90
53 054.853357	39.23526	0.00218	0.04908	1.081999	48.10
54 169.797044	39.21023	0.00163	0.04642	1.106171	54.90
54 171.841675	39.21269	0.00283	0.03670	1.091107	35.40
54 231.707362	39.20796	0.00387	0.04717	1.024483	26.90
54 254.558935	39.20832	0.00247	0.03249	1.065047	38.00
54 255.598697	39.20774	0.00204	0.03988	1.088968	44.80
54 257.602953	39.21209	0.00214	0.04304	1.140604	42.50
54 258.605074	39.20594	0.00182	0.03554	1.139446	48.90
54 527.870224	39.20544	0.00206	0.03445	1.035098	44.80
54 558.763909	39.21444	0.00208	0.05435	1.086478	44.00
54 582.711795	39.21463	0.00152	0.04262	1.093295	57.80
54 612.681536	39.21956	0.00235	0.04062	1.043033	40.20
54 670.539688	39.23551	0.00196	0.04093	1.008780	47.30
54 687.513837	39.22915	0.00248	0.03922	1.123480	39.30
54 872.814746	39.24546	0.00190	0.04367	1.075356	47.40
54 930.706596	39.25341	0.00161	0.03461	1.080127	55.00
54 930.791436	39.25556	0.00162	0.04109	1.114953	55.00
54 931.701621	39.25591	0.00190	0.04474	1.272736	47.80
55 013.555076	39.23016	0.00191	0.04243	0.964742	48.20
55 017.548011	39.23467	0.00111	0.03545	1.015099	80.40
55 019.520542	39.22898	0.00239	0.03698	1.044004	40.30
55 229.818454	39.22747	0.00147	0.04034	0.936748	60.10
55 266.818669	39.22445	0.00157	0.03614	0.975268	56.50
55 290.775088	39.22982	0.00143	0.04935	1.081048	61.90
55 303.643575	39.22369	0.00289	0.02272	0.936411	34.10
55 311.831470	39.23308	0.00177	0.03440	1.046885	53.60
55 313.584639	39.23289	0.00257	0.03924	1.007605	37.90
55 315.777596	39.23394	0.00284	0.04650	0.815662	35.70
55 321.615314	39.22823	0.00246	0.03302	1.053027	39.40
55 326.594991	39.23243	0.00222	0.04859	1.101968	43.10
55 334.643626	39.22892	0.00338	0.05334	1.024856	31.10
55 338.667081	39.23282	0.00291	0.04506	1.007748	34.80
55 350.643184	39.23347	0.00241	0.03681	1.051212	40.30
55 358.657970	39.23032	0.00252	0.05919	1.077452	39.40
55 358.668097	39.22599	0.00287	0.04342	0.925699	35.80
55 375.502804	39.23396	0.00169	0.04900	1.061762	54.70
55 402.518558	39.23080	0.00561	0.00931	0.931513	22.20
55 408.526208	39.23014	0.00304	0.04389	0.992615	34.00
55 414.476222	39.23212	0.00201	0.04906	0.961157	48.00
55 425.469477	39.23312	0.00157	0.03978	0.920064	59.30
55 437.485285	39.23088	0.00302	0.03167	0.811507	34.90
55 443.485145	39.22965	0.00561	0.04462	1.042132	22.30
55 586.874738	39.22011	0.00169	0.03624	1.092483	55.00
55 672.667929	39.20730	0.00207	0.03167	1.085615	45.70
55 689.633239	39.20769	0.00155	0.05545	1.191228	59.10
55 691.763736	39.20173	0.00232	0.03523	1.082861	42.60
55 694.553894	39.20315	0.00189	0.03102	1.050578	49.50
55 728.518219	39.20413	0.00243	0.05858	1.186629	41.10
55 729.518201	39.20088	0.00201	0.05703	1.138445	47.30
55 749.499966	39.20142	0.00218	0.04478	1.176564	44.50
55 755.453622	39.19367	0.00310	0.02074	1.000829	34.00
55 772.474746	39.20061	0.01074	0.03613	1.138059	14.00
55 961.887747	39.19702	0.00181	0.04792	1.092375	52.60
55 964.807747	39.19658	0.00264	0.02703	1.069307	38.50
55 967.883196	39.19852	0.00130	0.04082	0.957865	70.70
56 023.756120	39.20292	0.00249	0.03843	1.141698	39.50
56 051.779397	39.20250	0.00155	0.03471	1.113070	59.20
56 054.529353	39.20143	0.00542	0.03528	1.129481	22.20
56 095.540186	39.20893	0.00313	0.04351	1.196871	33.60
56 168.478323	39.21476	0.00239	0.03947	1.225962	42.10
56 311.829678	39.21198	0.00165	0.05030	1.201069	58.70
56 312.850414	39.22693	0.02383	0.05976	–0.069866	7.50
56 320.839755	39.21498	0.00222	0.04133	1.141358	44.90
56 331.875251	39.20866	0.00177	0.05142	1.218641	55.50
56 369.743652	39.20569	0.00231	0.04073	1.275527	43.60
56 384.797775	39.20373	0.00231	0.04280	1.101498	43.10
56 412.732946	39.21537	0.00141	0.04831	1.215775	67.00
56 441.473126	39.21324	0.00305	0.05314	1.228108	34.50
56 679.874554	39.25385	0.00304	0.05325	1.276441	34.80
56 716.890700	39.25921	0.00231	0.03585	1.285259	43.50
56 730.869538	39.25383	0.00216	0.03982	1.172956	45.40
56 740.776614	39.25155	0.00114	0.04124	1.346276	82.30
56 746.765923	39.25945	0.00232	0.03245	1.318461	43.30
56 755.780837	39.25554	0.00233	0.04692	1.246124	42.50

Notes. S/N gives the signal-to-noise value per pixel at 550 nm.

Table 9. Radial-velocity measurements obtained with HARPS of BD -114672.

JD-2 400 000.	RV [km s^{-1}]	σ_{RV} [km s^{-1}]	BIS [km s^{-1}]	S_{MW}	S/N
53 577.638500	–87.34721	0.00236	0.04557	0.789306	39.30
53 579.641564	–87.33761	0.00207	0.02781	0.860043	43.80
53 862.818306	–87.33258	0.00207	0.04196	0.726725	44.10
53 864.809683	–87.32871	0.00179	0.03201	0.792391	49.80
53 870.791313	–87.33006	0.00133	0.03916	0.741974	65.50
54 174.902721	–87.32065	0.00183	0.02689	0.785526	49.90
54 392.497515	–87.31897	0.00192	0.03391	0.731616	47.30
54 556.888627	–87.32936	0.00151	0.03917	0.682344	57.60
54 582.832192	–87.32881	0.00168	0.02971	0.713436	52.50
54 609.771934	–87.32864	0.00137	0.03030	0.719046	63.50
54 609.838848	–87.33008	0.00166	0.03099	0.726367	54.10
54 671.713924	–87.33226	0.00178	0.03223	0.639844	50.90
54 686.586739	–87.33309	0.00135	0.03167	0.676599	65.20
54 720.559621	–87.33249	0.00173	0.03116	0.715382	51.50
54 722.595695	–87.33276	0.00169	0.03792	0.694008	53.50
54 931.904537	–87.34475	0.00162	0.03805	0.704232	54.50
55 013.714941	–87.34569	0.00184	0.04073	0.715019	49.30
55 091.538435	–87.33488	0.00506	0.03153	0.851032	22.40
55 260.902428	–87.34112	0.00146	0.04076	0.846135	61.50
55 313.832975	–87.33405	0.00297	0.03782	0.774970	34.20
55 337.901286	–87.34011	0.00339	0.03820	0.766106	31.70
55 358.865074	–87.33887	0.00197	0.04183	0.770427	49.20
55 375.722713	–87.34447	0.00278	0.02731	0.767840	36.30
55 388.651469	–87.33068	0.00204	0.02902	0.775941	47.30
55 404.661284	–87.34487	0.00286	0.03101	0.790423	35.70
55 408.734655	–87.33044	0.00294	0.02235	0.786248	35.20
55 438.630840	–87.33190	0.00175	0.03596	0.717285	54.00
55 491.507904	–87.32843	0.00208	0.03192	0.779473	46.60
55 685.943023	–87.31756	0.00193	0.04043	0.802957	50.50
56 023.850615	–87.31882	0.00169	0.03319	1.012264	55.90
56 023.890306	–87.32552	0.00222	0.04285	0.919467	44.00
56 054.757351	–87.31429	0.00569	0.04935	0.808981	21.50
56 079.794608	–87.31693	0.00196	0.03802	0.772068	49.30
56 388.921992	–87.33923	0.00318	0.04078	0.746579	33.00
56 453.797518	–87.34113	0.00559	0.03034	0.658049	21.80
56 457.785445	–87.33738	0.00329	0.04085	0.782907	32.30
56 474.667467	–87.33169	0.00448	0.05626	0.680633	25.40
56 497.755121	–87.33078	0.00253	0.02928	0.804986	39.80
56 564.479769	–87.34215	0.00190	0.02707	0.618980	51.00
56 749.896171	–87.34789	0.00270	0.04503	0.731619	37.30

Notes. S/N gives the signal-to-noise value per pixel at 550 nm.